https://doi.org/10.15407/ujpe63.6.531

W. THONGPAN,[1,2] T. KUMPIKA,[2] E. KANTARAK,[2] A. PANTHAWAN,[2]
P. POOSEEKHEAW,[2] P. SINGJAI,[2,3,4] A. TUANTRANONT,[4,5] W. THONGSUWAN[2,3,4]

[1] PhD's Degree Program in Applied Physics, Faculty of Science, Chiang Mai University
(239, Huay Kaew Road, Muang, Chiang Mai 50200, Thailand)
[2] Department of Physics and Materials Science, Faculty of Science, Chiang Mai University
(239, Huay Kaew Road, Muang, Chiang Mai 50200, Thailand)
[3] Materials Science Research Center, Faculty of Science, Chiang Mai University
(239, Huay Kaew Road, Muang, Chiang Mai 50200, Thailand; e-mail: wiradej.t@cmu.ac.th)
[4] Center of Advanced Materials of Printed Electronics and Sensors,
Materials Science Research Center, Faculty of Science, Chiang Mai University
(Chiang Mai 50200, Thailand)
[5] Thailand Organic and Printed Electronics Innovation Center,
National Electronics and Computer Technology Center,
National Science and Technology, Development Agency
(Klong Luang, Pathumthani 12120, Thailand)

EXTERNAL-ELECTRIC-FIELD-ENHANCED UNIFORMITY AND DEPOSITION RATE OF A TiO_2 FILM PREPARED BY THE SPARKING PROCESS

We have used an external electric field to increase both the uniformity and deposition rate of TiO_2 films. The experiment is carried out by sparking-off titanium wires with a high dc voltage of 1 kV (field E_{int} = 10 kV/cm) and a limited current of 3 mA. The external electric fields (E_{ext}) of 3, 6, and 9 kV/cm were applied to the sparking system for 1–5 hours. The as-deposited film morphology was characterized by scanning electron microscopy. The results clearly show that the films are only deposited on the external electric field area. Furthermore, the deposition rate of the films increased from 40.7% to 77.8% in the presence of the external electric field of 9 kV/cm. The effects of an external electric field on both the deposition rate and uniformity of films are investigated and described.

Keywords: TiO_2 film, sparking process, external electric fields.

1. Introduction

Over the past few decades, nanostructures are attracted the increasing attention due to their potential application in various fields [1–5]. Various physical and chemical processes such as the gas evaporation [6–8], hydrothermal [9–11], sputtering [12, 13], and sol-gel method [14–17] have been used to synthesize nanomaterials. However, these techniques are usually expensive and complicated. The physical processes are generally carried out in a high vacuum system, while the chemical processes require the use of solvents or chemical precursors, which is time consuming and costly. Thus, there is an obvious need for an alternative. The sparking process is an effective, inexpensive, and rapid technique to synthesize high-quality nanoparticles and thin films. Using this process, films can be deposited directly onto a substrate without the need for a vacuum system [18, 19].

The sparking process was started at our laboratory in 2007 to synthesize high-quality small-size nanopar-

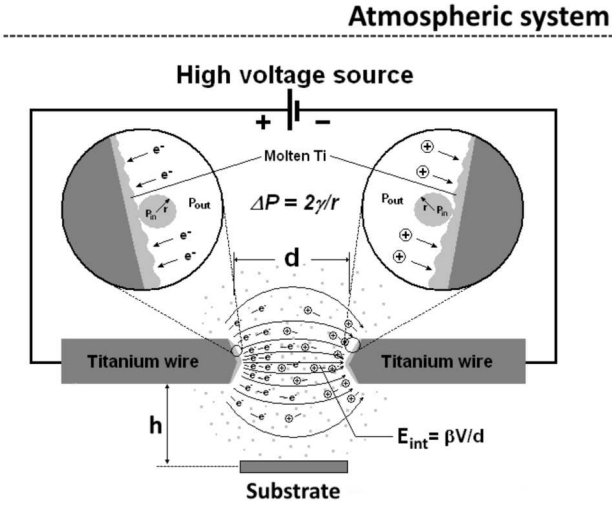

Fig. 1. Schematic diagram of the preparation of nanoparticles, by using the sparking process

ticles and highly porous films [20]. All metal nanoparticles such as, for example, Ti, Au, Ag, Al, V, Zn, Co, Ni, and Mo ones can be prepared, by using this process. Due to the large surface-to-volume ratio and the size effects on the nanoscale, nanoparticles exhibit novel properties with a prospect to their potential applications in nanoelectronics [21, 22], sensor technology [23–25], catalysts [26, 27], hydrogen storage [28, 29], and solar technology [30–32].

In 2008, the sparking process was studied by A. Schmidt-Ott and his co-worker at the Delft University of Technology, Netherlands [33–35]. This technique, which they called spark discharge, produces nanoparticles with the use of the ablation of electrodes. After the extinction of a spark, the vapor plume is cooled by the adiabatic expansion formed in the vicinity of the electrodes and condenses to form atomic clusters, nanoparticles, and their agglomerates. Finally, an inert gas carries the formed particles away from the electrodes and deposits on the substrate [36]. This process can control the size of the particles, by varying the initial energy and the gas flow rate.

The sparking process was carried out by applying a high dc voltage to metallic tips and caused a high electric field ($E_{\rm int} \sim 10$ kV/cm), which correlates to $E \propto V/d$, as shown in Fig. 1. The high pressure and temperature on the tip surfaces were generated by the bombardment of electrons and ions within a very short time [37]. This caused the melting of the metallic tip surfaces, and the droplets of nanoparticles dropped off the tip surface onto a substrate. The particle size can be varied by adjusting the applied voltage, which is described with the Young–Laplace equation, i.e. $\Delta P = 2\gamma/r$, where r is the radius of curvature, γ is the surface energy of the molten metallic tip, and ΔP is the pressure difference between the inside ($P_{\rm in}$) and the outside ($P_{\rm out}$) of the particle [38]. Therefore, the higher the applied voltage, the smaller the synthesized nanoparticles.

To explain more the mechanics of formation of particles by the sparking process, they start with applied energy ($E_{\rm app}$) to the wires, which is the source of nanoparticles. Then the energy was separated into the energy loss ($E_{\rm loss}$) to an environment and the melting energy for metal wires as described below by Eq. (1). The mass (m) of a particle from one spark can be estimated with Eq. (2) [39]

$$E_{\rm app} = E_{\rm loss} + mc_p(T_m - T) + mL_f, \tag{1}$$

$$m = \frac{E_{\rm app} - E_{\rm loss}}{c_p(T_m - T) + L_f}. \tag{2}$$

The first term in the numerator represents the energy of sparks. The second term denotes the heat loss by radiation and conduction. The terms in the denominator represent the energy required to heat the metallic tips to their melting point, where c_p and L_f are the heat capacity and the heat of fusion of metallic tips. This equation shows the mass of a particle in the sparking process depending on the input energy of sparks and wire properties. Therefore, if we want to increase the deposition rate of films, we should increase the input energy of sparks.

The sparking process will synthesize high-quality small-size particles and high porous films in the inexpensive rapid way. However, one significant limitation in the sparking process is the inability to control the direction of nanoparticles. This causes the low yield and nonuniformity of deposited films on a substrate, as shown in Fig. 1. In fact, most nanoparticles which dropped off the metallic tips had an electric charge, and then they will move under the action of the internal electric field ($E_{\rm int}$) around sparking tips [38]. Therefore, the external electric fields ($E_{\rm ext}$) could be applied to confine nanoparticles on the substrate for increasing the deposition rate and uniformity of the film. In this paper, the effects of external electric fields on the deposition rate and uniformity of films will be investigated and discussed.

2. Experimental

A schematic view of the sparking apparatus is shown in Fig. 2. The experiment was carried out by sparking off titanium wires (ϕ0.25 mm, purity 99.5%, Advent Research materials, Ltd) with a high DC voltage of ∼1 kV (equal to the internal electric field, $E_{\text{int}} \sim$ ∼ 10 kV/cm) and a limited current of ∼3 mA. The wires were then placed horizontally at the center of two external electrodes with the 1-mm spacing (d) of wire tips. The repetition rate of sparks and the spark pulse duration were fixed at 6.2 Hz and 0.16 s, respectively. The external electric fields (E_{ext}) of 3, 6, and 9 kV/cm which produced by high DC voltages of 4.5, 9, and 13.5 kV on external electrodes were applied to the sparking system for 1–5 h. The Cu plates (ϕ3 cm, purity 99.0%) were used as external electrodes, and the cathode was placed 0.75 cm above the sparking tips, while the anode was 0.75 cm below the tips in an atmospheric system at room temperature. In this study, a Cu plate $10 \times 10 \times 1$ mm^3 in size was used as a substrate, which was placed at the top electrode for avoid the deposition of large particles on the substrate due to the gravity.

The as-deposited film morphologies were characterized by scanning electron microscopy (SEM, JEOL JSM 6335F). The deposition rates of the films were investigated by a weighing machine (resolution 0.00001 g, Mettler Toledo).

3. Results and Discussion

Figure 3, *a, c* shows the top-view of the SEM images of films as-deposited by the sparking without an external electric field (no E_{ext}) and the sparking with an external electric field (E_{ext}) at 9 kV/cm, respectively. This comparison clearly shows the high-yield and regularly arranged structures of deposited films on a substrate when the external electric field is applied. This is a promising result for an enhancement of the film morphology. The high coverage of a film represents the uniform particle dispersion on substrates. The high-magnification SEM shows as-deposited films with a fluffy morphology due to an irregular stacking of primary nanoparticles and the formation of agglomerated large particles, as shown in Fig. 3, *b, d*. The agglomeration or the sticking of particles to one another is a natural phenomenon of nanoparticles. Our previous papers [18, 19], showed that the as-deposited particles produced by the sparking process are small with primary sizes of about 1–5 nm. Compared with those works, the primary sizes of particles could be still the same, because we use the same condition for the sparking process and improve only the applied external electric field. However, the size of agglomerated particles is decreased under the action of the applied external electric field. Therefore, the external electric field had a significant effect on the yield, uniformity, and size of agglomerated particles of the films.

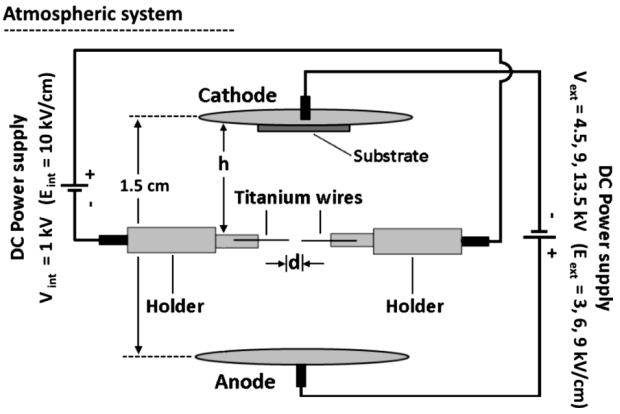

Fig. 2. Schematic diagram of the sparking apparatus

The relationship between the film mass and the total mass loss of a wire as a function of the time at various external electric fields is shown in Fig. 4. It is revealed that the mass of a film increases with the time and the external electric field. The masses of films observed were approximately 0.57, 0.80, 0.99, and 1.05 mg with applied external electric fields of 0, 3, 6, and 9 kV/cm for 5 h, respectively. In other words, the deposition rates for films were approximately 0.11, 0.16, 0.20, and 0.21 mg/h, respectively. The deposition rate for the sparking with the applied E_{ext} was clearly higher than without it. Therefore, this result can confirm that the external electric field had the effect to increase the yield and deposition rates of films. Moreover, the film produced without applied E_{ext} shows an inhomogeneous morphology, as compared with that with the applied E_{ext}, as shown on the photo in Fig. 4. The area of the substrate with deposited particles becomes white, which is characteristic of titanium particles.

The graph in Fig. 4 shows that the total mass of nanoparticles synthesized by this process increases with the duration of the sparking, which is repre-

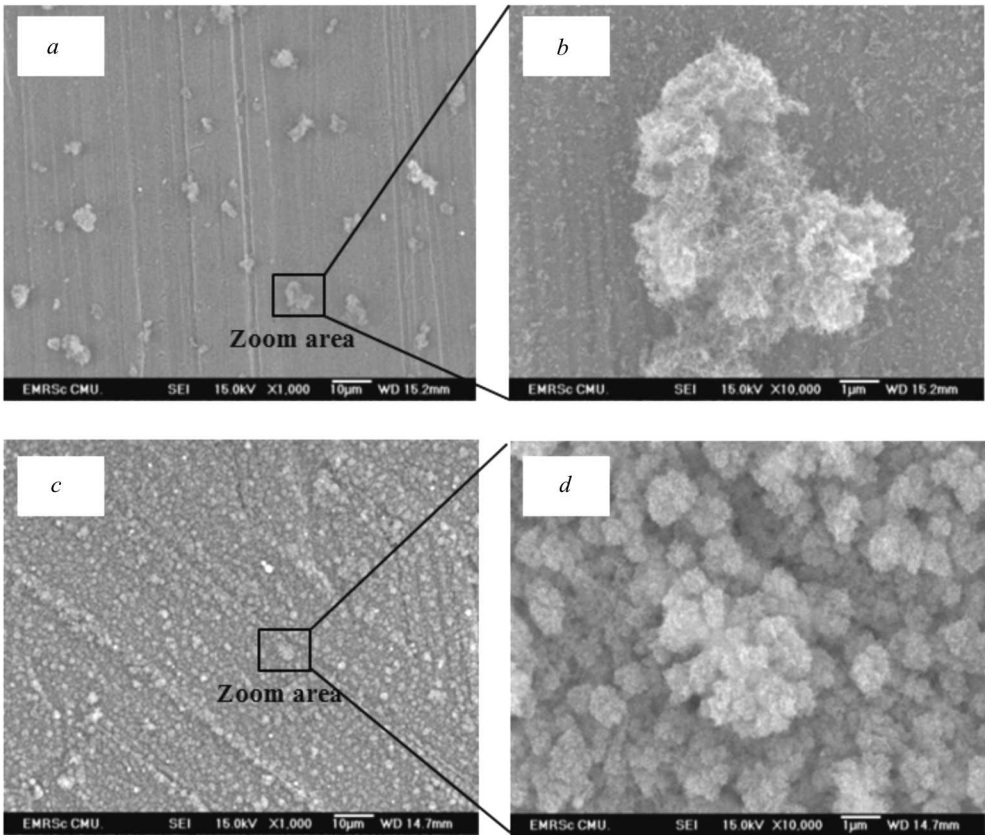

Fig. 3. SEM images of as-deposited thin films by sparking without external electric field (no E_{ext}) (a–b), sparking with external electric field (E_{ext}) at 9 kV/cm for magnifications of 1,000 and 10,000, respectively, (c–d)

sented by the mass loss of both wires, as shown by a blue line. This gives the synthesis rate for the sparking process to be 0.27 mg/h. Thus, the percent yield of the deposited film on a substrate compared with the total mass in the sparking process was 40.7, 59.2, 74.1, and 77.8%, respectively (see Table). The results in this table show that the deposition rate increases with the applied external electric field and is almost doubled at 9 kV/cm. This would reduce both the time and cost for the production.

Correlations of the mass, deposition rate, and percent yield of films

Sample	Mass of a film (mg) after 5 h	Mean deposition rate (mg/h)	% yield of a film
Without E_{ext}	0.57	0.11	40.7
$E_{\text{ext}} = 3$ kV/cm	0.80	0.16	59.2
$E_{\text{ext}} = 6$ kV/cm	0.99	0.20	74.1
$E_{\text{ext}} = 9$ kV/cm	1.05	0.21	77.8

It is of interest that the mass loss of a wire increases linearly with the time, whereas the mass of a film increased exponentially, which could be due to the thickness of films, as shown in Fig. 5. The electric field between electrodes will decrease, as the TiO_2 film becomes thicker, which is described by the equation $E = \frac{1}{\kappa}E_0$, where κ is the dielectric constant (86 for titanium). Therefore, the electrical force of the particles between the parallel electrodes is reduced, which correlates to $F \propto qE$. As a result, to deposition rate for films on a substrate decreases by more times.

The relationship between the deposition rate of films as a function of the time at various external electric fields is shown in Fig. 6. Normally, the deposition rate of films should be a constant, as a result of the mass loss of a wire. This graph shows a linear

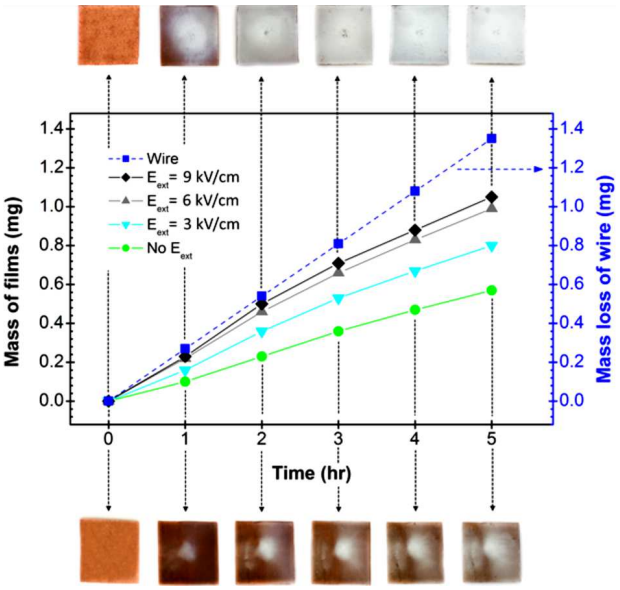

Fig. 4. Plot of the mass of films and the mass loss of a wire as a function of the time at various external electric fields and the photo of a film

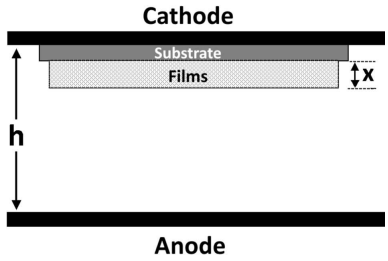

Fig. 5. Schematic diagram of the film thickness correlation with the external electric field

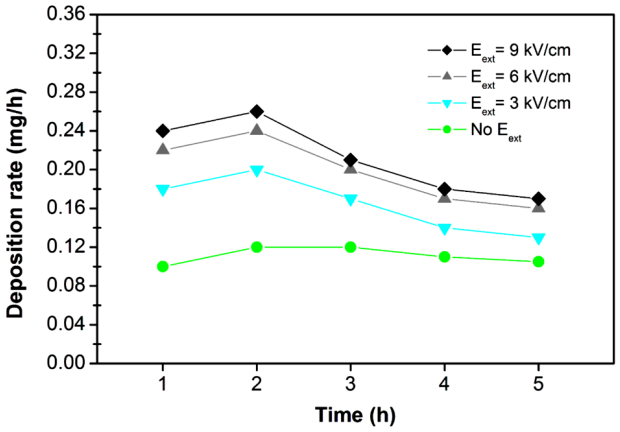

Fig. 6. Plot of the deposition rate of films as a function of the time for various external electric fields

trend for the deposition rates of films prepared by the sparking without applied E_{ext} and a downtrend for those prepared with applied E_{ext}. This result is related to the effect of the increasing thickness of a film on a reduction of the electric field between parallel electrodes, as mentioned before. Except at 2 h, the result shows that the deposition rate of films increases. This could be the effect of that the particles yet not covered all the substrate. Thus, the external electric field does not decrease at this point, as was mentioned in the previous paper [18]. If the lines of the deposition rates of films were continuous, they would approach each other and meet the line with the sparking process without applied E_{ext}.

We note that this graph shows that the sparking with applied external electric fields of 6 and 9 kV/cm has similar results for the deposition rate, which shows that this point was the maximum limit for applied external electric fields. Therefore, most nanoparticles in the sparking process were confined to the substrate with an applied external electric field of 6 kV/cm. If higher external electric fields were applied to the sparking process, the number of nanoparticles formed still remained the same.

4. Conclusions

The enhancement in the uniformity and deposition rate of TiO_2 films in the sparking process was successfully realized, by applying an external electric field. The application of external electric fields leads to the higher yield, higher deposition rate, and regularly arranged structure of a film deposited on the substrate. Deposition rates of approximately 0.11, 0.16, 0.20, and 0.21 mg/h were obtained by the sparking process with external electric fields (E_{ext}) of 0, 3, 6, and 9 kV/cm applied for 5 h, respectively. In other words, the percent yields of films deposited on the substrate comparable with the total mass loss due to the sparking were 40.7, 59.2, 74.1, and 77.8%, respectively. The optimized value of the applied external electric field was 6 kV/cm, for which most of the nanoparticles from the sparking process were confined to the substrate.

We thank the National Research University Project under Thailand's office of the Commission on Higher Education (CHE), the Science Achievement Scholarship of Thailand (SAST), the Thailand Research Fund (TRF), the Graduate School in Chiang Mai

University (GSCMU), and the Center of Excellence in Advanced Materials for Printed Electronics and Sensors (CMU-NECTECH) for the financial support.

1. P. Hou, J. Qian, X. Cheng, S.P. Shah. Effects of the pozzolanic reactivity of nano SiO_2 on cement-based materials. *Cement & Concrete Compos.* **55**, 250 (2015).
2. R. Gong, G. Chen. Preparation and application of functionalized nano drug carriers. *Saudi Pharm. J.* **24**, 254 (2016).
3. P. Subalakshmi, A. Sivashanmugam. CuO nano hexagons an efficient energy storage material for Li-ion battery application. *J. Alloys Comp.* **690**, 523 (2017).
4. P. Catald, I.S. Bayer, R. Cingolani, S. Marras, R. Chellali, A. Athanassiou. Thermochromic superhydrophobic surface. *Sci. Rep.* **6**, 1 (2016).
5. A. Soam, P. Kavle, A. Kumbhar, R.O. Dusane. Performance enhancement of micro-supercapacitor by coating of graphene on silicon nanowires at room temperature. *Current Appl. Phys.* **17**, 314 (2017).
6. P.R. Somani, S.P. Somani, M. Umeno. Planer nanographenes from camphor by CVD. *Chem. Phys. Lett.* **430**, 56 (2006).
7. G. Deokar, J. Avila, I.R. Colambo, J.L. Codron, C. Boyaval, E. Galopin, M.C. Asensio, D. Vignaud. Towards high quality CVD graphene growth and transfer. *Carbon* **89**, 82 (2015).
8. N.K. Park, G.B. Han, J.D. Lee, S.O. Ryu, T.J. Lee, W.C. Chang, C.H. Chang. The growth of ZnO nano-wire by a thermal evaporation method with very small amount of oxygen. *Current Appl. Phys.* **6S1**, e176 (2006).
9. N. Donga, F. Hea, J. Xina, Q. Wanga, Z. Leia, B. Sua. A novel one-step hydrothermal method to prepare $CoFe_2O_4$/graphene-like carbons magnetic separable adsorbent. *Materials Research Bulletin* **80**, 186 (2016).
10. T. Jiang, Y. Wang, D. Meng, X. Wu, J. Wang, J. Chen. Controllable fabrication of CuO nanostructure by hydrothermal method and its properties. *Appl. Surf. Sci.* **311**, 602 (2014).
11. T. Hu, Y. Su, I.R. Baxendale, J. Tan, H. Tang, L. Xiao, F. Zheng, P. Ning. Adjust band gap of IATO nanoparticles to obtain desirable optical property by one-step hydrothermal oxidation. *Current Appl. Phys.* **17**, 584 (2017).
12. J. Sicha, J. Musil, M. Meissner, R. Cerstvy. Nanostructure of photocatalytic TiO_2 films sputtered at temperatures below 200 °C. *Appl. Surf. Sci.* **254**, 3793 (2008).
13. Y.T. Kim, J. Park, J. Choi. Sputter-deposited ZnO thin films consisting of nano-networks for binder-free dye-sensitized solar cells. *Current Appl. Phys.* **13**, 381 (2013).
14. X. Li, X. Quan, C. Kutal. Synthesis and photocatalytic properties of quantum confined titanium dioxide nanoparticle. *Scripta Mater.* **50**, 499 (2004).
15. L. Duan, X. Zhao,Y. Zhang, H. Shen, R. Liu. Fabrication of flexible Al-doped ZnO films via sol–gel method. *Mater. Lett.* **162**, 199 (2016).
16. Z. Xin, M. Lei, W. Jian-gang, Z. Hui-min. Investigation on ultrathin titanium oxide films synthesized by surfacesol–gel method. *Optik* **127**, 2780 (2016).
17. K.J. Chen, F.Y. Hung, S.J. Chang, S.J. Young, Z.S. Hu. Effects of crystallization on the optical properties of ZnO nano-pillar thin films by sol-gel method. *Current Appl. Phys.* **11**, 1243 (2011).
18. W. Thongsuwan, T. Kumpika, P. Singjai. Effect of high roughness on a long aging time of superhydrophilic TiO_2 nanoparticle thin films. *Current Appl. Phys.* **11**, 1237 (2011).
19. W. Thongsuwan, T. Kumpika, P. Singjai. Photocatalytic property of colloidal TiO_2 nanoparticles prepared by sparking process. *Current Appl. Phys.* **8**, 563 (2008).
20. T. Kumpika, W. Thongsuwan, P. Singjai. Atomic force microscopy imaging of ZnO nanodots deposited on quartz by sparking off different tip shapes. *Surf. Interface Anal.* **39**, 58 (2007).
21. E. Zaminpayma, P. Nayebi. Electronic and electrical properties of silicon nanowire single wall carbon nanotube junction as a nanoelectronic switch. *Comput. Mater. Sci.* **110**, 198 (2015).
22. R.E. Triambulo, J.W. Park. Electronic properties of transparent nano-composite electrodes for application in flexible electronics. *Current Appl. Phys.* **15**, S12 (2015).
23. X. Jiao, L. Zhang, Y. Lv, Y. Su. A new alcohols sensor based on cataluminescence on nano-CdS. *Sensors and Actuators B* **186**, 750 (2013).
24. S.Y. Lee, M. Takai, H.M. Kim, K. Ishihara. Preparation of nano-structured titanium oxide film for biosensor substrate by wet corrosion process. *Current Appl. Phys.* **9**, e266 (2009).
25. H. Kim, S. Jang. AlGaN/GaN HEMT based hydrogen sensor with platinum nanonetwork gate electrode. *Current Appl. Phys.* **13**, 1746 (2013).
26. Z. Ren, Y. Guo, P.X. Gao, Nano-array based monolithic catalysts: Concept, rational materials design and tunable catalytic performance. *Catalysis Today* **258**, 441 (2015).
27. R. Mimouni, A. Souissi, A. Madouri, K. Boubaker, M. Amlouk. High photocatalytic efficiency and stability of chromium-indium codoped ZnO thin films under sunlight irradiation for water purification development purposes. *Current Appl. Phys.* **17**, 1058 (2017).
28. W. Chen, Y. Zhu, C. Yang, J. Zhang, M. Li, L. Li. Significantly improved electrochemical hydrogen storage properties of magnesium nickel hydride modified with nano-nickel. *J. of Power Sources* **280**, 132 (2015).
29. C. Zhang, J. Li, C. Shi, C. He, E. Liu, N. Zhao. Effect of Ni, Fe and Fe-Ni alloy catalysts on the synthesis of metal contained carbon nano-onions and studies of their electrochemical hydrogen storage properties. *J. Energy Chem.* **23**, 324 (2014).
30. Z. Chen, X. Zhang, J. Fang, J. Liang, X. Liang, J. Sun, D. Zhang, N. Wang, H. Zhao, X. Chen, Q. Huang, C. Wei, Y. Zhao. Enhancement in electrical performance of thin-

film silicon solar cells based on a micro- and nano-textured zinc oxide electrodes. *Appl. Energy* **135**, 158 (2014).

31. M. Wanit, J. Yeo, S.J. Hong, Y.D. Suh, S.H. Ko, D. Lee, C.P. Grigoropoulos. ZnO nano-tree growth study for high efficiency solar cell. *Energy Procedia* **14**, 1093 (2012).
32. J. Jang, M. Kim, Y. Kim, K. Kim, S.J. Baik, H. Lee, J.C. Lee. Three-dimensional a-Si:H thin-film solar cells with silver nano-rod back electrodes. *Current Appl. Phys.* **14**, 637 (2014).
33. S. Schwyn, A. Schmidt-Ott. Aerosol generation by spark discharge. *Aerosol Sci.* **19**, 639 (1988).
34. N. S. Tabrizi, M. Ullmann, V. A. Vons, U. Lafont, A. Schmidt-Ott. Generation of nanoparticles by spark discharge. *Nanopart. Res.* **11**, 315 (2009).
35. T.V. Pfeiffer, J. Feng, A. Schmidt-Ott. New developments in spark production of nanoparticles. *Adv. Powder Techn.* **25**, 56 (2014).
36. E.J. Lehtinen, M. R. Zachariah. Energy accumulation in nanoparticle collision and coalescence processes. *Aerosol Sci.* **33**, 357 (2002).
37. R. Reinmann, M. Akram. Temporal investigation of a fast spark discharge in chemically inert gases. *Phys. D Appl. Phys.* **30**, 1125 (1997).
38. R.J. Hunter. *Introduction to Modern Colloid Science* (Oxford Univ. Press, 1993).
39. F. Llewellyn Jones. Electrode erosion by spark discharges. *Appl. Phys.* **1**, 60 (1950).

Received 29.12.17

В. Тонгпен, Т. Кумпіка,
Е. Кантарак, А. Пантаван, П. Пусіхів,
П. Сінджай, А. Туантранонт, В. Тонгсуван

ПОЛІПШЕННЯ ОДНОРІДНОСТІ І ЗБІЛЬШЕННЯ ШВИДКОСТІ УТВОРЕННЯ ІСКРОВИМ РОЗРЯДОМ TiO_2 ПЛІВОК У ЗОВНІШНЬОМУ ЕЛЕКТРИЧНОМУ ПОЛІ

Р е з ю м е

Зовнішнє електричне поле застосовано для збільшення однорідності і швидкості утворення плівок TiO_2. Експеримент виконано іскровим розрядом з Ті дротів при сталій напрузі 1 кВ (поле $E_{\rm int}$ = 10 кВ/см) і невеликому струмі 3 мА. Система іскрового розряду перебувала в зовнішніх електричних полях ($E_{\rm ext}$) 3, 6, і 9 кВ/см від 1 до 5 годин. Морфологія тільки що приготовлених плівок визначалася методом растрової електронної мікроскопії. Показано, що плівки формуються тільки в області дії зовнішнього електричного поля. У зовнішньому електричному полі 9 кВ/см швидкість утворення плівок збільшилася з 40,7% до 77,8%. Досліджено і описано дію зовнішнього електричного поля на швидкість утворення і однорідність плівок.